



CHORUS

This is the accepted manuscript made available via CHORUS. The article has been published as:

Catalyst-particle configurations: From nanowires to carbon nanotubes

Qian Zhang, Stephen H. Davis, and Peter W. Voorhees
Phys. Rev. E **96**, 022802 — Published 16 August 2017

DOI: [10.1103/PhysRevE.96.022802](https://doi.org/10.1103/PhysRevE.96.022802)

Catalyst-particle configurations: From nanowires to carbon nanotubes

Qian Zhang* and Stephen H. Davis†

*Department of Engineering Sciences and Applied Mathematics,
Northwestern University, 2145 Sheridan Road, Evanston, Illinois 60208-3125, USA*

Peter W. Voorhees‡

*Department of Materials Science and Engineering, Northwestern University,
2225 Campus Drive, Evanston, Illinois 60208-3030, USA*

(Dated: July 24, 2017)

Surface-energy minimization is used to study capillary effects that determine the stable configurations of (liquid or solid) particles atop tubes or wires. The results give allowable ranges for the volume (V_c) of the particles as function of the inner and outer radii of the tubes, R_I and R_o , respectively. When $R_I/R_o = 0$, the object is a nanowire. When $R_I/R_o = 1$, it is a single-wall carbon nanotube (SWCNT). When $0 < R_I/R_o < 1$, it can be thought of as a multi-wall carbon nanotube (MWCNT). Moreover, the transition paths among different configurations are studied. These results suggest possible mechanisms for the reshaping of the “pear-like” catalyst particles in carbon nanotubes that oscillate across a local energy-maximum points with respect to the position of the lower interface in the inner wall.

I. INTRODUCTION

Since identified in 1991 by Sumio Iijima [1], carbon nanotubes (CNTs) have captured the attention of researchers due to their useful chemical and physical properties[2]. Catalytic chemical vapor deposition (CCVD) is a most promising method of their synthesis because of its low cost and scalable technique for bulk production. However, mass production of defect-free CNTs remains a challenge. The root of solving this problem is to understand the mechanisms of growth. There are many parameters involved in the synthesizing processes, involving hydrocarbons, catalysts, heat, pressure, gas-flow rates, deposition times and reactor geometries. The easiest controllable parameter is the catalyst volume. Moreover, it is suggested in many experiments [3, 4] that the CNT morphology (outer and inner diameters, the number of walls) has a close relationship with the volumes of the catalyst particles required.

Many attempts have been made to estimate optimal conditions for controlling the configurations of CNTs via the sizes of the catalyst particles both experimentally and theoretically. A. Gohiera et al. [5] observe that the ratio between diameters of the catalyst and the single-wall carbon nanotubes (SWCNTs) is close to a constant and independent of other experimental conditions. Schebarchov et al. [6], using a simple model and molecular-dynamic simulation, finds that nonwetting molten nanoparticles below a critical size can enter the interior of single wall CNTs in the process of base growth. In the growth of multi-wall carbon nanotubes (MWCNTs), the catalyst particles seem to display pear-like shapes which oscillate in time. It is shown by en-

vironmental transmission electron microscopy (ETEM) that the CNT morphology is governed by the dynamic reshaping of the catalyst particles [7–10].

The droplet penetration into capillary tubes, pipettes [6, 11–14] or pores [15] has been investigated both theoretically and numerically in the past. In all the previous theoretical analyses, it has been assumed that the droplet contacts the tube inlet [6, 11–14], or spreads along the top face [15]. This assumption is valid for thin tube walls or SWCNTs. However, for MWCNTs, this assumption is insufficient in the tip-growth process because the catalyst particle could contact the tube at the outer edge. Thus, in the present paper, the more general case is considered; a tube with outer and inner radii (R_o and R_I where $0 \leq R_I \leq R_o$ and $0 < R_o < \infty$), respectively. The protruding catalyst particle can be pinned at the inner or outer edge or the top face of the tube (see Fig. 3, 4). The analysis covers the withdrawal and uptaking processes of droplets from the CNTs, which is different from the works that focus on the penetration process [6, 11–15]. Thus, the present analysis also augments the theory to dynamic processes and possible equilibrium states of liquid droplets atop capillary tubes, especially for tubes in which the thickness of the wall cannot be neglected. *Note: Configurations can only be stable if the energy is locally minimum and the contact angles (both with the tube inlet and the tube outlet) are in admissible ranges.*

In summary, in the present paper, drops atop tubes of inner and outer radii R_I and R_o , respectively, are examined for stability by using surface-energy minimization techniques. The surface-energy model that we use has been used frequently before, e.g. see Ref. [16]. We use this because we aim to study the stable conditions of solid/liquid particles and energy minimization is a direct path to them. Moreover, only axisymmetric cases are considered given that these are the most commonly observed shapes. When $\rho \triangleq R_I/R_o = 0$, the tube becomes a nanowire which grows by the Vapor-Liquid-Solid(VLS)

* qian.zhang.jennifer@northwestern.edu

† sdavis@northwestern.edu

‡ p-voorhees@northwestern.edu

method and the drop is liquid. When $\rho > 0$, the tube becomes a tube like a SWCNT or MWCNT and the particle can be in solid or crystal state as shown in Ref. [17]. In this case, our results are related to tip growth of both SWCNTs and MWCNTs. It is found that there is a minimum size of particle for tip-growth to proceed. All the results are expressed in terms of ρ , $\bar{R} = V_c^{1/3}/R_o$ and the wetting conditions via Young's contact angle θ_Y . The transition among different equilibrium states for the catalyst particle is tracked allowing one to understand the possible mechanisms for the reshaping process of the catalyst particle in tip-growth of CNTs or wires. Finally, it is worth mentioning that the method we are using for tip-growth and conclusions we have obtained for tip-growth in this paper are also applicable to that of base growth cases because at the nanoscale gravity is negligible compared with surface tension.

II. RESULTS AND DISCUSSIONS

Fig. 1 shows a typical tip-growth process of a CNT. As the hydrocarbon decomposes on the catalyst particle and the carbon atoms diffuse to the bottom of the catalyst, the whole catalyst is pushed off the substrate (From the stage shown in Fig. 1(b) to Fig. 1(c)). Afterwards, the catalyst particle rises and then sits atop the CNT. As long as the top of the catalyst is open for fresh hydrocarbon decomposition, the CNT continues to grow longer as shown in Fig. 1(d). It is observed in many experiments that the lower meniscus of catalyst particle shown in Fig. 1(c) oscillates during the growth process and that this oscillation influences the growth process of CNT significantly. Our objective is to investigate the mechanisms leading to each axisymmetric state of catalyst particle in the tip-growing process and to understand the influences of the properties of the catalyst particle on the configuration of the growing carbon nanotube.

In the model, surface-energy minimization of each state shown in Fig. 1 is considered. For the convenience of illustration, Fig. 2(b) shows a tip-growth process in which a catalyst particle lies atop a growing tube, where γ_{SV} is the interfacial energy density between the wall of the CNT and the vapor, γ_{SL} is the interfacial energy density between the wall and the catalyst particle, and γ_{LV} is the interfacial energy density between the vapor and the catalyst particle. The equilibrium Young's angle θ_Y at the contact line (three-phase line) formed by the particle, the vapor and the wall defined in Fig. 2(c) by

$$\gamma_{LV} \cos \theta_Y = \gamma_{SV} - \gamma_{SL}. \quad (1)$$

Notice that if the surface of the particle contacts the inner wall, then $\phi = \theta_Y$. On the other hand, if the upper surface contacts the top face of the tube, then $\theta = \theta_Y$. Because the tube and the catalyst particle are in the nano scale, it is reasonable to assume that the force of gravity applied on the catalyst particle can be neglected compared with the interfacial forces.

In addition, according to the analysis in Appendix II D, we only consider cases where $\theta_Y > \pi/2$ in the following. If the upper surface of the catalyst particle is pinned at the outer edge of the tube with angle θ , see Fig. 2(b), and the lower surface of the catalyst particle is pinned at the inner edge of the tube with angle ϕ as shown in Fig. 2(b), the admissible angle range of θ and ϕ are

$$\theta_Y \leq \theta \leq \pi, \quad (2)$$

$$\frac{\pi}{2} \leq \phi \leq \theta_Y. \quad (3)$$

In tip growth, the tube system shown in Fig. 2(b), there are seven parameters:

- The interfacial energy densities: γ_{SV} , γ_{SL} and γ_{LV} (which determine θ_Y);
- The volume of the catalyst particle: V_c ;
- The size of the carbon nanotube characterized by the outer (R_o) and inner diameters (R_I) and the length (H). The thickness of the wall is defined by $d = R_o - R_I$.

Let the lengths in the system be scaled by R_o and the energy density in the system by γ_{LV} so the total energy of the system is scaled by $\gamma_{LV} R_o^2$. Define

$$\bar{R} = V_c^{1/3}/R_o, \quad \bar{H} = H/R_o, \quad \rho = R_I/R_o. \quad (4)$$

Then, in order to let the particle contact the inner wall, it has to satisfy $V_c \geq 4\pi R_I^3/3$, so that

$$\bar{R} \geq 1.612\rho. \quad (5)$$

Here, ρ measures of the number of walls in the multiwall CNT. In the cases discussed in Fig. 1(b) and 1(c), $0 < \rho \leq 1$ while $\rho = 0$ in the case shown in Fig. 1(d) describes a solid nanowire.

Reference case: consider a specific case in which $\theta_Y = 2\pi/3$ with the volume of catalyst particle and CNT as given in [7, 9]. $V_c = 230\text{nm}^3$ with radii $R_I = 1.35\text{nm}$ and $R_o = 1.6\text{nm}$, consistent with Eq. (5). We shall refer future results to this "standard" case.

The remainder of this paper is organized as follows. In Section II A, we discuss the conditions for the catalyst particle to leave the substrate, which is the stage shown from Fig. 1(b) to Fig. 1(c). Instability of "pear-like" catalyst shapes (shown in Fig. 3) and the conditions for the transition among configurations shown in Fig. 3 and Fig. 4 in the stage shown from Fig. 1(c) to Fig. 1(d) are presented in Section II B. The influences of the size of catalyst on the geometry and morphology of the tube are considered in Section II C. In what follows, there are three types of configurations discussed. Those labeled E have particles encapsulated within the tube, those labeled P are "pear-like" shapes, those labeled C are caps atop the wire/tube.

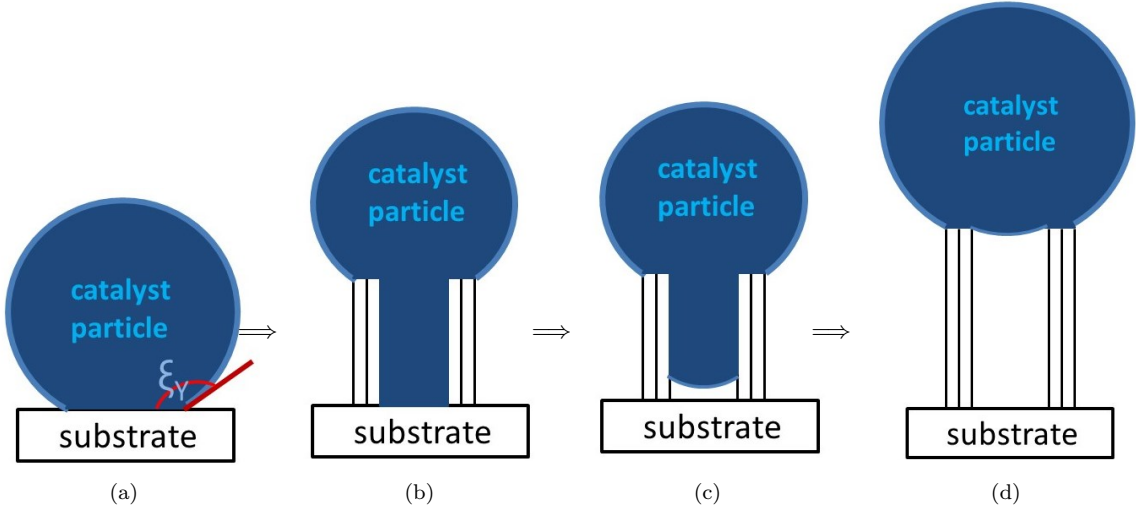


FIG. 1. Typical tip-growth process. (a) A catalyst particle is placed on a substrate; (b) to (c): As the hydrocarbon decomposes on the catalyst particle and the carbon atoms diffuse to the bottom of the catalyst particle, the whole catalyst particle is pushed off the substrate; (d) The catalyst particle moves up and sits atop the CNT.

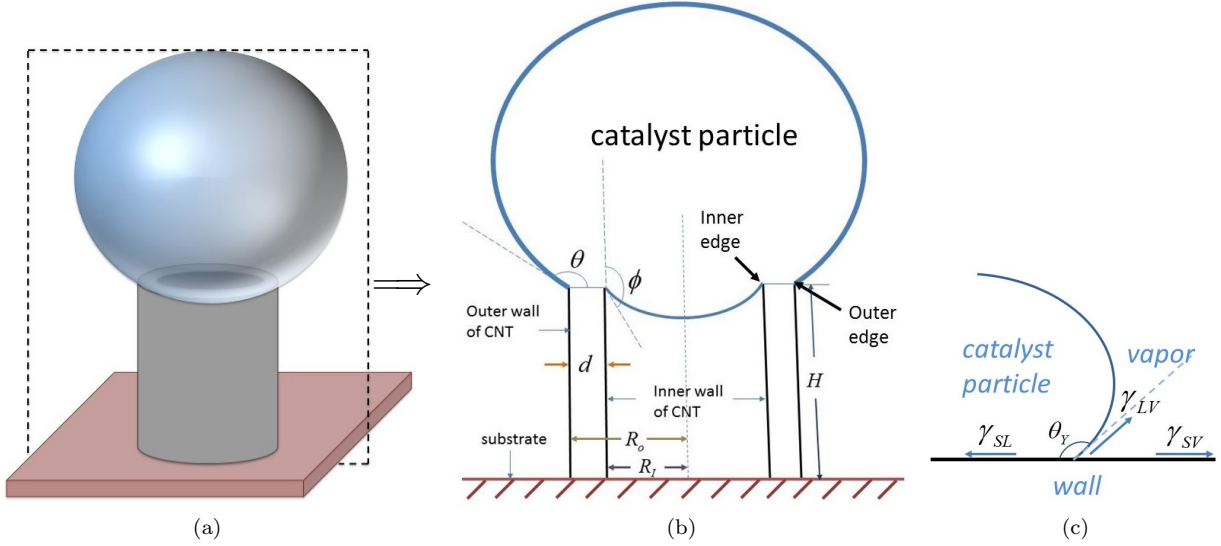


FIG. 2. (a) Sketch of a catalyst particle at the tip of growing MWtube; (b) Vertical cross-section of Fig. 2(a); (c) Sketch of the equilibrium Young's angle. Here, "wall" includes the outer wall, the inner wall and the top of the tube.

A. Conditions for the catalyst particle to leave the substrate

In Fig. 1(b), suppose that the tube is very short and the catalyst particle still contacts the substrate. If the interfacial energy density between the substrate and the vapor is γ_{SuV} and the interfacial energy density between the substrate and the catalyst particle is γ_{SuL} , the wettability of the catalyst on the substrate can be described by the contact angle ξ_Y ; see Fig. 1(a), where

$$\gamma_{LV} \cos \xi_Y = \gamma_{SuV} - \gamma_{SuL}. \quad (6)$$

The energy difference between the case of touching the substrate (shown in Fig. 1(b)) and not touching it (shown in Fig. 1(c)) is

$$\Delta E = E_{touch} - E_{untouch} \leq -\pi R_I^2 \gamma_{LV} (1 + \cos \xi_Y) \leq 0.$$

Thus, the catalyst *always prefers* contact with the substrate. In order for the catalyst to detach, it must be subjected to some perturbation. Moreover, in order to let the catalyst detach from the substrate, the perturbation is smaller the hydrophobic substrates than hydrophilic substrates. This is consistent with most experimental observations that the adhesion force between the catalyst particle and the substrate influences the growth mode

(tip-growth or base growth) of the tube.

B. Instability of “pear-like” catalyst shapes in the tube growth

In Fig. 1(c), the catalyst has detached from the substrate, the top of the catalyst particle is atop the tube, and the bottom dips into the interior (as shown in Fig. 3). The contact angle at the inner wall between the bottom of the catalyst particle and the vapor is θ_Y . The distance between the inner edge of the tube and the contact line of the lower interface is defined by δ as shown in Fig. 3. d_i (in Fig. 3(b)) is the distance between the contact point of the upper interface with the top and the inner edge of the tube. Define $\bar{\delta} = \delta/R_o$ as the effective contact depth and $\bar{d}_i = d_i/R_o$ as the effective contact distance. This configuration is the “pear-like” shape which has been observed in many experiments on CNTs [7–10]. Because the catalyst is sitting atop the tube, there are three possible positions for the upper surface as shown in Fig. 3. In this section, $0 < \bar{d}_i \leq 1 - \rho$ and $\rho > 0$, $\bar{\delta} > 0$ because we are considering “pear-like” catalyst shapes.

Given H and $\delta \approx H$ at the instant the catalyst lifts from the substrate, different sizes of catalysts can lead to different configurations. If

$$\bar{R} \geq [v(\theta_Y) + \rho^3 v(\theta_Y - \frac{\pi}{2}) + \pi \bar{H} \rho^2]^{\frac{1}{3}}, \quad (7)$$

where the first term of the right-hand side is the volume of the catalyst particle above the tube, the sum of the last two terms is the volume of the catalyst particle within the tube, and

$$v(\theta) = \frac{\pi(1 - \cos \theta)(2 + \cos \theta)}{3 \sin \theta(1 + \cos \theta)},$$

the upper interface contacts the outer edge of the tube, as shown in Fig. 3(a), and the contact angle between the upper interface of catalyst particle and vapor and top face is θ , $\theta_Y \leq \theta \leq \pi$. If

$$\begin{aligned} & \{\rho^3 [v(\theta_Y) + v(\theta_Y - \frac{\pi}{2})] + \pi \bar{H} \rho^2\}^{\frac{1}{3}} < \bar{R} \\ & < [v(\theta_Y) + \rho^3 v(\theta_Y - \frac{\pi}{2}) + \pi \bar{H} \rho^2]^{\frac{1}{3}}, \end{aligned} \quad (8)$$

the upper surface contacts the top face of the tube, as shown in Fig. 3(b), and the contact angle between the

upper surface and the top is θ_Y . If

$$\begin{aligned} & [2v(\theta_Y - \frac{\pi}{2})\rho^3 + \pi \bar{H} \rho^2]^{\frac{1}{3}} \leq \bar{R} \\ & \leq \{\rho^3 [v(\theta_Y) + v(\theta_Y - \frac{\pi}{2})] + \pi \bar{H} \rho^2\}^{\frac{1}{3}}, \end{aligned} \quad (9)$$

and the upper surface contacts the inner edge of the tube, as shown in Fig. 3(c), and the contact angle between the upper surface and the top is θ_i , $\theta_Y - \pi/2 \leq \theta_i \leq \theta_Y$. On the other hand, given the volume V_c of the catalyst, the catalyst can evolve to any of the three states by changing the position of the lower meniscus, i.e., the value of $\bar{\delta}$ (or \bar{H} in Eq. (7)-(9)).

In the reference case, in order to have a part protruding from the tube, the catalyst particle has to detach from the substrate at $\bar{H} \leq 25.14$. In particular, if the catalyst particle detaches from the substrate at $\bar{H} \leq 22.8$, the catalyst particle is shown in Fig. 3(a); if the catalyst particle detaches from the substrate at $22.8 < \bar{H} \leq 23.8$, the catalyst particle is shown in Fig. 3(b); if the catalyst particle detaches from the substrate at $23.8 < \bar{H} \leq 25.14$, the catalyst particle is shown in Fig. 3(c).

P1: The upper meniscus contacts the outer edge of the tube [Fig. 3(a)]

Because $\bar{H} > 0$, then in order to include all the possible values of \bar{R} in this state, we consider

$$\bar{R} > [v(\theta_Y) + \rho^3 v(\theta_Y - \frac{\pi}{2})]^{\frac{1}{3}} \triangleq V_A(\theta_Y, \rho), \quad (10)$$

where $V_A^3(\theta_Y, \rho)$ represents the dimensionless volume of the catalyst particle when $\bar{\delta} = 0$ and $\theta = \theta_Y$. Given the size of the tube and volume of the catalyst, the catalyst state depends on θ and δ . In particular, if the catalyst particle leaves the substrate when the length of the tube is H , then $\delta \approx H$. The dimensionless volume of the catalyst particle is then

$$\bar{R}^3(\theta, \bar{\delta}) = v(\theta) + \rho^3 v(\theta_Y - \frac{\pi}{2}) + \pi \bar{\delta} \rho^2. \quad (11)$$

Define a scaled total energy

$$\mathcal{E} = E_{total}/\gamma_{LV} R_o^2,$$

where E_{total} is the total surface energy of the system under consideration. The energy of the system is

$$\frac{1}{2\pi} \mathcal{E}(\theta, \bar{\delta}) = \left[\frac{1}{1 + \cos \theta} + \rho^2 \frac{1}{1 + \sin \theta_Y} \right] + \frac{\gamma_{SV}}{\gamma_{LV}} (\rho + 1) \bar{H} - \bar{\delta} \rho \cos \theta_Y + \frac{1}{2} \frac{\gamma_{SL}}{\gamma_{LV}} [1 - \rho^2], \quad (12)$$

where $\bar{\delta} \geq 0$ and $\theta_Y \leq \theta \leq \theta_Y + \pi/2$. Thus,

$$\frac{d\mathcal{E}}{d\bar{\delta}} = \rho \cos \theta_Y \left(\frac{r}{R} - 1 \right), \quad (13)$$

where R and r are the radii of curvature of the upper and the lower surfaces, respectively. It is obvious that

$$\frac{d\mathcal{E}}{d\bar{\delta}} = 0, \text{ and } \frac{d^2\mathcal{E}}{d\bar{\delta}^2} \leq 0, \text{ when } R = r,$$

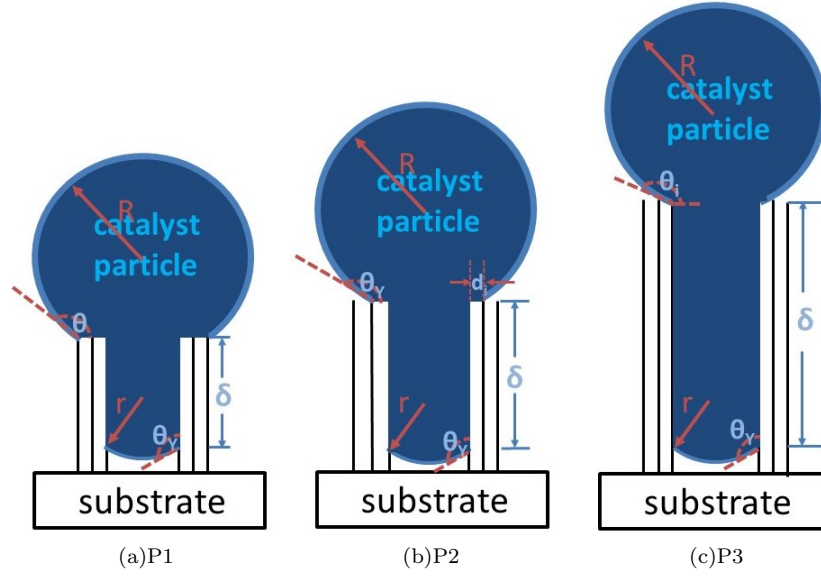


FIG. 3. “Pear-like” shapes of the catalyst particle. (a) P1: Upper meniscus contacts outer edge of tube and lower contacts the inner wall of the tube; (b) P2: Upper meniscus contacts top of tube and lower meniscus contacts inner wall of the tube; (c) P3: Upper meniscus contacts inner edge of tube and lower meniscus contacts inner wall of the tube.

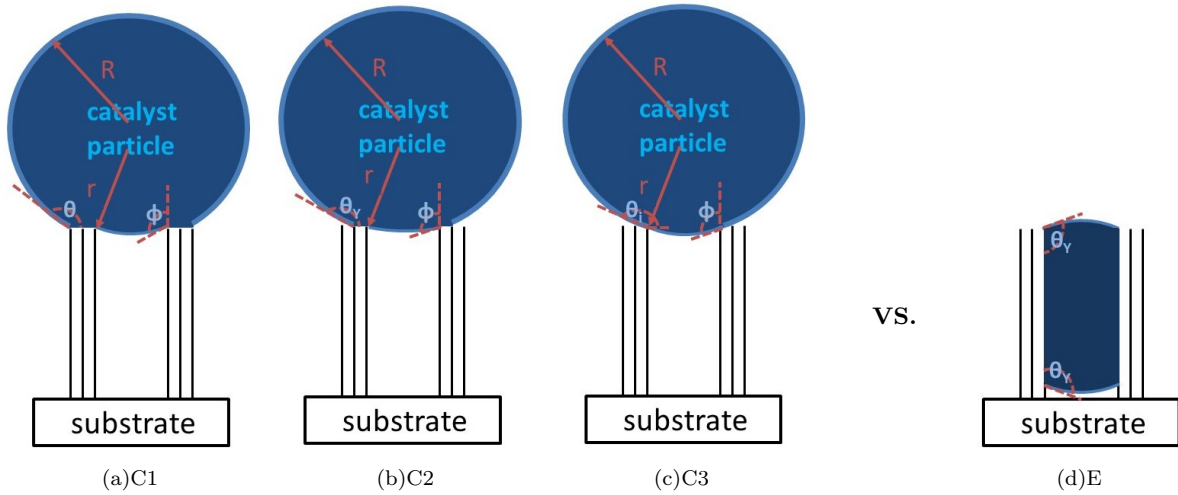


FIG. 4. Possible stable shapes of the catalyst particle. (a) C1: Upper meniscus contacts outer edge of tube; (b) C2: Upper meniscus contacts the top of tube and lower meniscus contacts the inner edge of the tube; (c) C3: Upper meniscus contacts the inner edge of tube and lower meniscus contacting inner edge of the tube; (d) E: The catalyst particle is encapsulated in the tube.

which implies the energy is maximum at $R = r$. Moreover, consider the admissible angle range of θ , $\theta_Y \leq \theta \leq \theta_Y + \pi/2$, if $\rho \leq \cot(\pi - \theta_Y)$,

$$\frac{d\mathcal{E}}{d\bar{\delta}} \geq \rho \cos(\pi - \theta_Y)[1 - \rho \tan(\pi - \theta_Y)] \geq 0.$$

Thus, the particle will always evolve to the state shown in Fig. 4(a) in which the lower surface contacts the inner edge and the upper meniscus contacts the outer edge of the tube. The above discussion is summarized in Fig. 5.

In the following, take $\theta_Y = 2\pi/3$, and identify two different regimes shown in Fig. 5(b) under the conditions that $\rho > \cot(\pi - \theta_Y)$ and $\bar{R} > V_A$.

$(\rho, \bar{R}) = (0.8, 3.0)$ is taken as the representative case for the regime colored light blue. Through the energy profile shown in Fig. 5(c) (the light blue curve), it is observed that there exists a local maximum at around $\bar{\delta} = 5 (\triangleq \bar{\delta}_0)$, which implies that the stable state of the particle is determined by the initial position of the lower surface. If $\bar{\delta} < \bar{\delta}_0$, it will evolve to a state shown in Fig. 4(a). If $\bar{\delta} > \bar{\delta}_0$, it will evolve to a state shown in Fig.

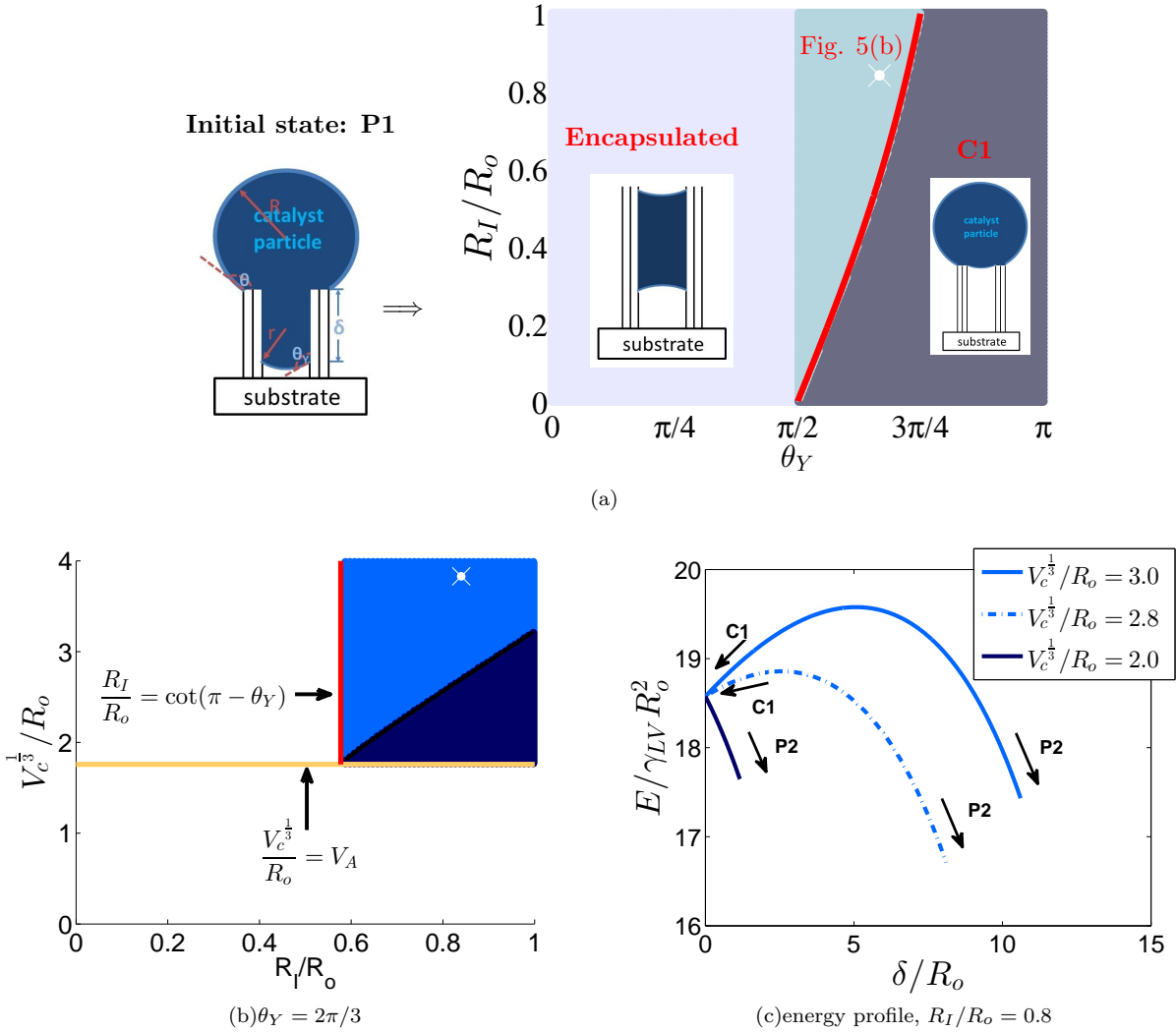


FIG. 5. With initial state shown in Fig. 3(a) named P1, (a) $(\theta_Y, R_I/R_o) = (\theta_Y, \rho)$ map of different situations, when $V_c^{1/3}/R_o \geq V_A(\theta_Y, R_I/R_o)$. Gray: Evolution to C1 shown in Fig. 4(a). Purple: Evolution to E shown in Fig. 4(d). Green: Discussed in detail in Fig. 5(b). The red line is $R_I/R_o = \cot(\pi - \theta_Y)$. The white point represents the reference case. (b) $(R_I/R_o, V_c^{1/3}/R_o) = (\rho, \bar{R})$ map of different states with $\theta_Y = 2\pi/3$. The line between blue and dark blue regions is Eq. (14). The white point represents the reference case. (c) The representative energy profiles of different regions shown in Fig. 5(b). The energy profile with $(V_c^{1/3}/R_o, R_I/R_o) = (\bar{R}, \rho) = (3.0, 0.8)$ and $(V_c^{1/3}/R_o, R_I/R_o) = (\bar{R}, \rho) = (2.8, 0.8)$ represent the blue region. The energy profile with $(V_c^{1/3}/R_o, R_I/R_o) = (\bar{R}, \rho) = (2.0, 0.8)$ represents the dark blue region. The right end of each energy profile is the position δ/R_o such that $\theta = \theta_Y$.

3(b) when \bar{H} is large enough. If \bar{H} is not large enough, the catalyst particle will return to the state shown in Fig. 1(b).

Moreover, a small perturbation around $\bar{\delta}_0$ may introduce oscillations of the part of the particle of the inner wall of the tube, which is a typical phenomenon observed in the experiments of tube growth [7, 8, 10], this small perturbation can be a thermal fluctuation where $k_B T / \gamma_{LV} R_o^2 \approx 10^{-1} \sim 10^{-2}$. Since the energy barriers are a small fraction of $k_B T$, it is highly likely that the system will not be localized in one energy minimum, but oscillate between them. $(\rho, \bar{R}) = (0.8, 2.8)$ is also

taken as the representative case for the regime colored light blue in Fig. 5(b). Compare the cases with $\bar{R} = 3.0$ and $\bar{R} = 2.8$, Fig. 5(c) shows that the oscillation of the catalyst particle inside the tube should be easier in the later case when subjecting to small perturbations. In sum, within the blue region, the closer (ρ, \bar{R}) to the line between the blue region and dark-blue region, the easier for the catalyst particle to oscillate. It worth mentioning that we have not analyzed possible oscillations but only mention their occurrence.

In the reference case, if the catalyst particle detaches from the substrate at $\bar{H} < 16.54$, it will evolve to state

C1, see Fig. 4(a), because $\theta_Y = 2\pi/3$, $\rho = 0.84$ and $\bar{R} = 3.83$ and (ρ, \bar{R}) is in the light blue region shown in Fig. 5(b). Similarly, if the catalyst particle detaches from the substrate at $\bar{H} > 16.54$, the catalyst particle will evolve to state P2 or the state shown in Fig. 1(b). If the system is subjected to perturbations and detaches from the substrate at $\bar{H} \approx 16.54$, the lower meniscus of the catalyst particle may oscillate within the tube.

Similarly, $(\rho, \bar{R}) = (0.8, 2.0)$ is taken as the representative case for the regime colored dark blue. The energy profile shows that the stable state of the catalyst will evolve to the case shown in Fig. 3(b) within the regime colored dark blue in Fig. 5(b).

In addition, the line between the light-blue region and dark-blue region in Fig. 5(b) is given by

$$\bar{R} = [v(\pi - \sin^{-1}(-\cos\theta_Y/\rho)) + \rho^3 v(\theta_Y - \frac{\pi}{2})]^{1/3} \quad (14)$$

because $d\mathcal{E}/d\bar{\delta} > 0$ at $\bar{\delta} = 0$, when $\theta > \pi - \sin^{-1}(-\cos\theta_Y/\rho)$.

P2: The upper meniscus contacts the top face of the tube [Fig. 3(b)]

Because $\bar{H} > 0$, then in order to include all the possible values of \bar{R} under this condition, consider

$$\bar{R} > \rho[v(\theta_Y) + v(\theta_Y - \frac{\pi}{2})]^{1/3} \triangleq V_B(\theta_Y, \rho), \quad (15)$$

where V_B^3 represents the dimensionless volume of the catalyst particle when $d_i = 0$ and $\delta = 0$ shown in Fig. 3(b).

Similarly to that in last section, if $\rho \geq \cot(\pi - \theta_Y)$, the state of the catalyst particle will evolve to state shown in Fig. 4(c). Furthermore, if $\tan(\pi - \theta_Y) \leq 1$, i.e., $\theta_Y \geq 3\pi/4$, the catalyst particle will evolve to the states shown in Figs. 4(b) or 4(a). The above discussion is summarized in Fig. 6.

In the reference case, if the catalyst particle detaches from the substrate at $22.8 < \bar{H} \leq 23.8$, the state of the catalyst particle is shown in Fig. 3(b) at the instant of leaving the substrate. Because $\rho = 0.84$ and $\theta_Y = 2\pi/3$ (shown in Fig. 6), it will evolve to the state shown in Fig. 3(c) or touch the substrate again according to the result above.

In the following, consider only $\rho \leq \cot(\pi - \theta_Y)$ and $\pi/2 \leq \theta_Y \leq 3\pi/4$. To investigate this case in detail, take $\theta_Y = 2\pi/3$ and identify three different regimes shown in Fig. 7(a).

$(\rho, \bar{R}) = (0.5, 3.0)$ is taken as the representative case for the regime colored yellow. Through the energy profile shown in Fig. 7(b), it is observed that there exists a local *maximum* at around $\bar{\delta} = 30 (\triangleq \bar{\delta}_0)$, which implies that the evolution of the state of the catalyst particle is determined by the initial position of the lower surface of the catalyst. If $\bar{\delta} < \bar{\delta}_0$, it will evolve to the state shown in Fig. 3(a), then evolve to state shown in Fig. 4(a)

according to the discussion in last section. If $\bar{\delta} > \bar{\delta}_0$, it will evolve to the state shown in Fig. 3(c).

Similarly, $(\rho, \bar{R}) = (0.5, 1.7)$ is taken as the representative case for the regime colored light blue in Fig. 7(a). If $\bar{\delta} < \bar{\delta}_0$, the catalyst particle will evolve to the state shown in Fig. 4(b). If $\bar{\delta} > \bar{\delta}_0$, it will evolve to a stable state as shown in Fig. 3(c). The right end of the energy profile stops at the position of $\bar{\delta}$ such that $\bar{d}_i = 0$. Moreover, the line between the light blue region and yellow region in Fig. 7(a) is

$$\bar{R} = [v(\theta_Y) + \rho^3 v(\theta_Y - \frac{\pi}{2})]^{1/3}. \quad (16)$$

This is because in the yellow region, the volume of the catalyst particle has to be large enough that $\bar{\delta} \geq 0$ when the upper surface reaches the corner of the outer wall of the tube and the top side of the tube, i.e., $\bar{d}_i + \rho = 1$.

Finally, $(\rho, \bar{R}) = (0.5, 1.5)$ is taken as the representative case for the regime colored red in Fig. 7(a). The energy profile (Fig. 7(d)) shows that the stable state of the catalyst will evolve to that shown in Fig. 3(c). The line between red and the light blue part is

$$\bar{R} = \rho[v(\theta_Y) \tan^3(\pi - \theta_Y) + v(\theta_Y - \frac{\pi}{2})]^{1/3} \quad (17)$$

because $d\mathcal{E}/d\bar{\delta} \geq 0$, at $\bar{\delta} = 0$ when $\bar{d}_i + \rho \geq \rho \tan(\pi - \theta_Y)$.

P3: The upper meniscus contacts the inner edge of the tube [Fig. 3(c)]

Because $\bar{H} > 0$, then in order to include all the possible values of \bar{R} under this condition, consider

$$\bar{R} \geq [2v(\theta_Y - \frac{\pi}{2})]^{1/3} \rho. \quad (18)$$

However, because it has been assumed that

$$\bar{R} \geq (\frac{4\pi}{3})^{1/3} \rho,$$

Eq. (18) is satisfied automatically. In addition,

$$\frac{d\mathcal{E}}{d\bar{\delta}} = \rho \cos\theta_Y (\frac{r}{R} - 1). \quad (19)$$

Here, $r/R = -\sin\theta_i/\cos\theta_Y$. It is obvious that

$$\frac{d\mathcal{E}}{d\bar{\delta}} \leq 0, \text{ when } \theta_Y \leq \frac{3\pi}{4}.$$

Moreover,

$$\frac{d\mathcal{E}}{d\bar{\delta}} = 0, \text{ and } \frac{d^2\mathcal{E}}{d\bar{\delta}^2} > 0, \text{ when } \theta_i = \theta_Y - \frac{\pi}{2}.$$

Thus, if $\pi/2 \leq \theta_Y \leq 3\pi/4$, the particle encapsulated within the tube as shown in Fig. 4(d) is the stable state.

In the reference case, if the catalyst particle detaches from the substrate at $23.8 < \bar{H} \leq 25.14$, the state of the

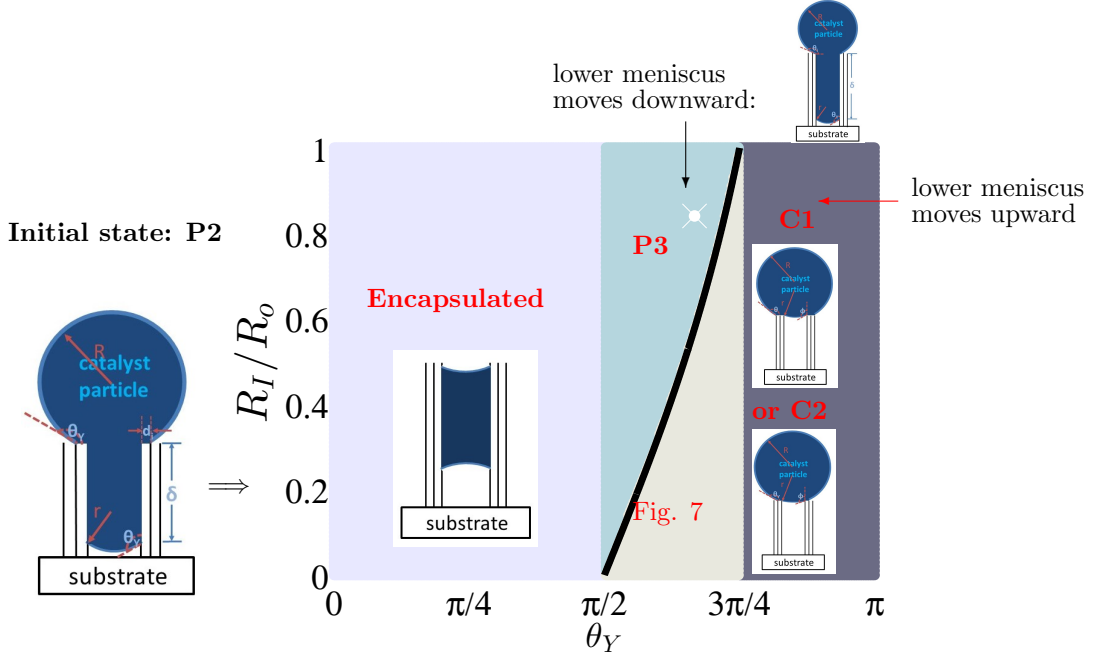


FIG. 6. With initial state shown in Fig. 3(b) named P2, $(\theta_Y, R_I/R_o)$ map of different states, when $V_c^{1/3}/R_o \geq V_B(\theta_Y, R_I/R_o)$. Gray: the state of catalyst particle evolves to C2 (Fig. 4(b)) or C1 (Fig. 4(a)). Green: the state of catalyst particle evolves to P3 (Fig. 3(c)). Purple: the state of catalyst particle evolves to E (Fig. 4(d)). Yellow: discussed in Fig. 7. The black line is $R_I/R_o = \cot(\pi - \theta_Y)$. The white point represents the reference case.

catalyst particle is shown in Fig. 3(c) at the instant of leaving the substrate. Because $\theta_Y = 2\pi/3$, it will evolve to the state shown in Fig. 4(d) or continue touching the substrate according to the result above.

However, if $\theta_Y > 3\pi/4$, there are two extrema. Besides the minimum point, $\theta_i = \theta_Y - \pi/2$, $\theta_i = 3\pi/2 - \theta_Y$ is the maximum point because

$$\frac{d\mathcal{E}}{d\bar{\delta}} = 0, \text{ and } \frac{d^2\mathcal{E}}{d\bar{\delta}^2} < 0, \text{ when } \theta_i = \frac{3\pi}{2} - \theta_Y.$$

Three regimes of (\bar{R}, ρ) are identified, as shown in Fig. 8(a), with $\theta_Y = 5\pi/6$.

If $\theta_i \leq 3\pi/2 - \theta_Y$ when $\bar{\delta} = 0$, the energy profile is shown in Fig. 8(d) [$(\bar{R}, \rho) = (0.5, 0.82)$ is taken as the representative point.] which implies the particle encapsulated within the tube is stable.

If $3\pi/2 - \theta_Y < \theta_i < \theta_Y$ when $\bar{\delta} = 0$, the stable state depends on the initial position of the lower surface of the catalyst in the tube. Taking $(\bar{R}, \rho) = (0.5, 1.1)$ as the representative case, it is easy to see from the energy profile, shown in Fig. 8(c), that the catalyst will evolve to the case shown in Fig. 4(c) when $\bar{\delta} < \bar{\delta}_0$, whereas the catalyst is encapsulated within the tube is stable when $\bar{\delta} > \bar{\delta}_0$.

If $\theta_i > \theta_Y$ when $\bar{\delta} = 0$, the stable state also depends on the initial position of the lower surface of the catalyst in the tube. Taking $(\bar{R}, \rho) = (0.5, 2.0)$ as the representative case (energy profile is shown in Fig. 8(b)), the situation is different from the former situation, because the catalyst

particle will evolve to the case shown in Fig. 3(b), then to the state shown in Fig. 4(a) or 4(b) according to the discussion in last section, when $\bar{\delta} < \bar{\delta}_0$.

In summary, the (\bar{R}, ρ) maps of the different situations with $\theta_Y = 5\pi/6$ are shown in Fig. 8(a). Furthermore, according to the analysis above, the line between yellow and red is given by

$$\bar{R} = [v(\theta_Y - \frac{\pi}{2}) + v(\frac{3\pi}{2} - \theta_Y)]^{\frac{1}{3}} \rho, \quad (20)$$

and the line between red and blue is given by

$$\bar{R} = [v(\theta_Y - \frac{\pi}{2}) + v(\theta_Y)]^{\frac{1}{3}} \rho. \quad (21)$$

First summary

- All the possible steady “pear-like” shapes are *unstable*. Pear-like shapes for the particle may oscillate along the inner wall of the tube as long as the lower surface detaches from the substrate when the length of the tube is near a critical value $\bar{\delta}_0$ and due to a small perturbations. That position is the location of the lower meniscus such that the upper and lower menisci have the same curvature.
- According to the discussion above, given \bar{R} and θ_Y , the evolution of the catalyst depends on the length H of the tube at the instant that the lower meniscus detaches from the substrate.

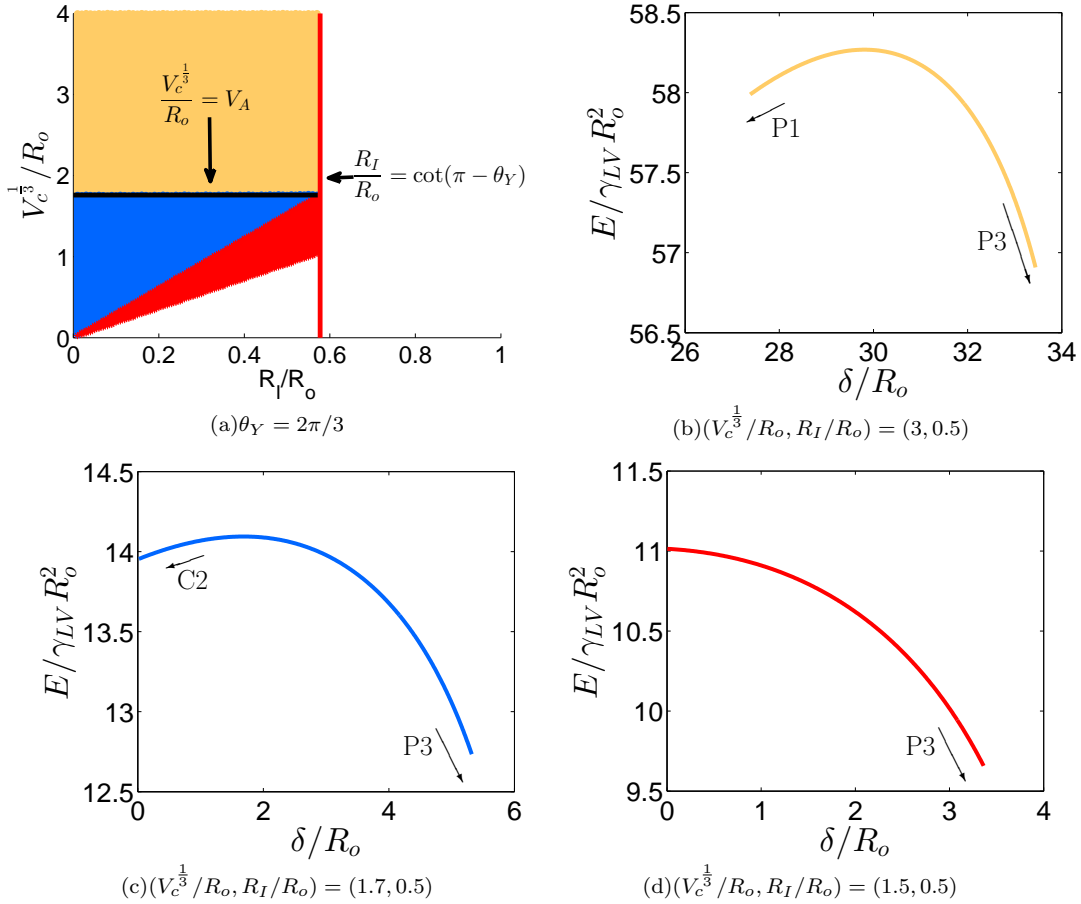


FIG. 7. With initial state shown in Fig. 3(b) named P2, (a) $(R_I/R_o, V_c^{1/3}/R_o) = (\rho, \bar{R})$ map of different states with $\theta_Y = 2\pi/3$. (b),(c) and (d) show the representative energy profiles corresponding to different regions shown in Fig. 7(a). (b) The energy profile with $(V_c^{1/3}/R_o, R_I/R_o) = (\bar{R}, \rho) = (3.0, 0.5)$ represents the yellow region. (c) The energy profile with $(V_c^{1/3}/R_o, R_I/R_o) = (\bar{R}, \rho) = (1.7, 0.5)$ represents the blue region. (d) The energy profile with $(V_c^{1/3}/R_o, R_I/R_o) = (\bar{R}, \rho) = (1.5, 0.5)$ represents the red region. The right end of energy profiles in Fig. 7(b), 7(c) and 7(d) is the position of δ/R_o such that $d_i/R_o = 0$. The left end of energy profile in Fig. 7(b) is the position of δ/R_o such that $d_i/R_o = 1 - R_I/R_o$. States P1 and P3 are shown in Fig. 3(a) and 3(c). State C2 is shown in Fig. 4(b).

(c) Generally speaking, if the volume of the catalyst is too small or the length H of the tube is too large at the instant that the lower menisci detaches from the substrate, the catalyst particle will become encapsulated within the tube and the growth process will cease.

C. Size of catalyst influences the size and morphology of the tube

According to the discussion in last section, the “pear-like” shapes will evolve to two kinds of configurations. One is that the whole catalyst is encapsulated within the tube, in which case the growth process stops. The other is that the lower meniscus of the catalyst contacts the inner edge, in which case the tube continues to grow as long as the catalyst’s top is open for hydrocarbon decomposition.

In this case, there are three different states possible as determined by the position of the upper meniscus shown in Fig. 4(a), 4(b) and 4(c).

According to the discussion above, the lower menisci contacts the inner wall of the tube with angle $\phi = \theta_Y$ at the instant of touching the inner edge, if

$$\bar{R} \geq [v(\theta_Y) + \rho^3 v(\theta_Y - \frac{\pi}{2})]^{1/3}, \quad (22)$$

the upper surface contacts the outer edge of the tube, as shown in Fig. 4(a), and the contact angle between the upper surface of catalyst and top is θ , $\theta_Y \leq \theta \leq \pi$; if

$$\rho[v(\theta_Y) + v(\theta_Y - \frac{\pi}{2})]^{1/3} < \bar{R} < [v(\theta_Y) + \rho^3 v(\theta_Y - \frac{\pi}{2})]^{1/3}, \quad (23)$$

the upper surface contacts the top of the tube, as shown in Fig. 4(b), and the contact angle between the upper

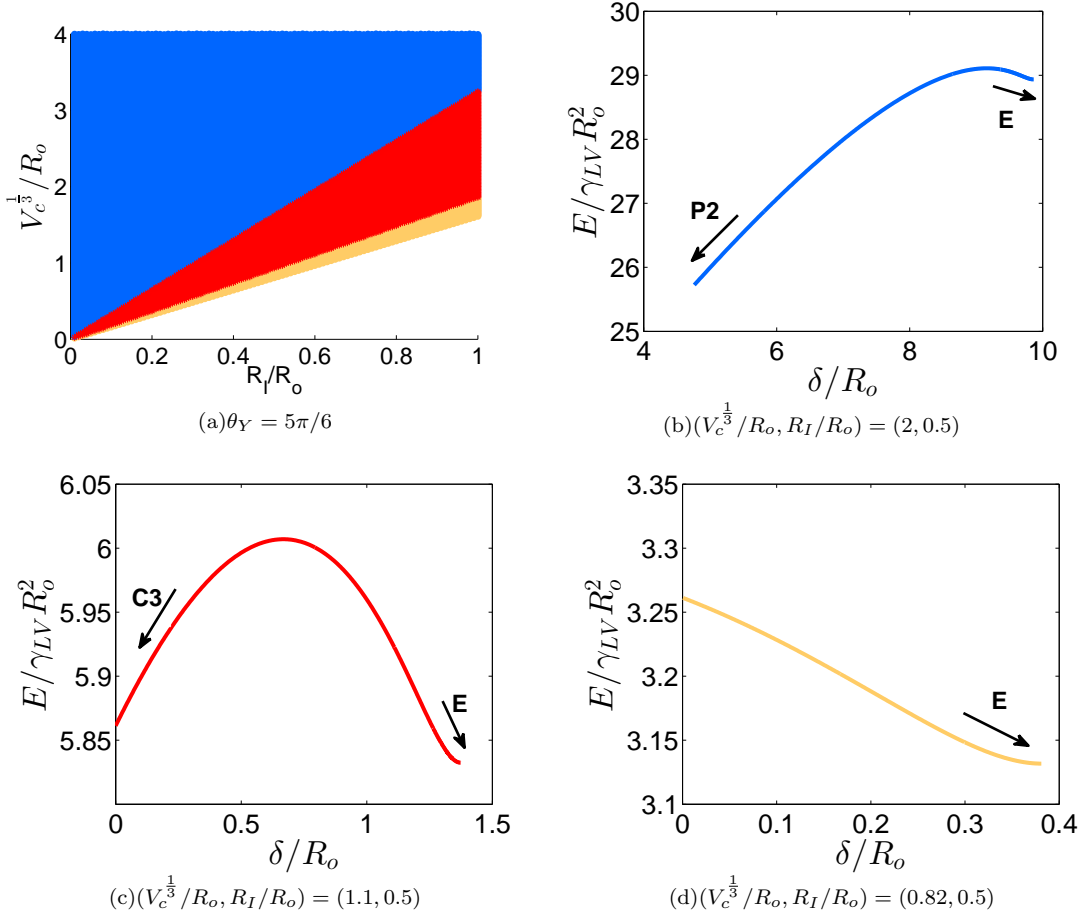


FIG. 8. With initial state shown in Fig. 3(c) named P3, (a) $(R_I/R_o, V_c^{1/3}/R_o) = (\bar{R}, \rho)$ map of different states with $\theta_Y = 5\pi/6$. (b), (c) and (d) show the representative energy profiles corresponding to different regions shown in Fig. 8(a). (b) Energy profile with $(V_c^{1/3}/R_o, R_I/R_o) = (\bar{R}, \rho) = (2, 0.5)$ represents the blue region. (c) Energy profile with $(V_c^{1/3}/R_o, R_I/R_o) = (\bar{R}, \rho) = (1.1, 0.5)$ represents the blue region. (d) Energy profile with $(V_c^{1/3}/R_o, R_I/R_o) = (\bar{R}, \rho) = (0.82, 0.5)$ represents the yellow region. The right end of energy profiles is the position of d_i/R_o such that $\delta/R_o = 0$. The left end of the energy profile in Fig. 8(b) is the position of δ/R_o when $\theta_i = \theta_Y$. The right end of the energy profiles are the position of δ/R_o when $\theta_i = \theta_Y - \pi/2$. States C3 and E are shown in Fig. 4(a) and 4(d). State P2 is shown in Fig. 3(b).

surface of catalyst and top is θ_Y ; if

$$\theta_i \leq \theta_Y.$$

$$\left(\frac{4\pi}{3}\right)^{\frac{1}{3}}\rho \leq \bar{R} \leq \rho[v(\theta_Y) + v(\theta_Y - \frac{\pi}{2})]^{\frac{1}{3}}, \quad (24)$$

the upper surface contacts the inner edge of the tube, as shown in Fig. 4(c), and the contact angle between the upper surface of the catalyst and top is θ_i , $\theta_Y - \pi/2 \leq$

C1: The upper meniscus contacts the outer edge of the tube [Fig. 4(a)]

In this case, the catalyst sits atop the tube with the upper surface contacting the outer edge and the lower contacting the inner edge. This configuration is observed in most tip-growing tube experiments [7, 8]. According to the analysis in Appendix: C1, if

$$\begin{aligned} (\bar{R}, \rho) \in \{ & (\bar{R}, \rho) \mid \bar{R} \geq [v(\theta_Y) + \rho^3 v(\frac{\pi}{2} - \cos^{-1}(\rho \sin \theta_Y))]^{\frac{1}{3}}, 0 \leq \rho \leq \cot(\pi - \theta_Y) \} \\ & \cap \{ (\bar{R}, \rho) \mid \bar{R} \geq [v(\pi - \sin^{-1}(-\cos \theta_Y / \rho)) + \rho^3 v(\theta_Y - \frac{\pi}{2})]^{\frac{1}{3}}, \cot(\pi - \theta_Y) \leq \rho \leq 1 \} \end{aligned} \quad (25)$$

for $\pi/2 < \theta_Y \leq 3\pi/4$ (see Fig. 9(a) as a representative case) and

$$(\bar{R}, \rho) \in \{(\bar{R}, \rho) \mid \bar{R} \geq [v(\theta_Y) + \rho^3 v(\frac{\pi}{2} - \cos^{-1}(\rho \sin \theta_Y))]^{\frac{1}{3}}, 0 \leq \rho \leq 1\} \quad (26)$$

for $3\pi/4 < \theta_Y < \pi$ (see Fig. 9(b) as a representative case), there always exist a stable state when the upper and the lower interfaces have the same curvature ($r = R$), and both ϕ and θ in Fig. 4(a) are in the admissible angle range shown in Eq. (3) and (2). Here, the contact angle between the upper meniscus of catalyst particle and the top is θ whereas the contact angle between the lower meniscus and the inner wall is ϕ , see Fig. 4(a). In addition, this result, Eq. (25) and (26) when $R_I = 0$, is also consistent with the discussion for stable states of

catalyst droplet on a (solid) nanowire in VLS nanowire growth in [16].

In the reference case, $\theta_Y = 2\pi/3$, $(\bar{R}, \rho) = (3.83, 0.84)$ is in the yellow region shown in Fig. 9(a). This implies that the catalyst particle will evolve to and stay at a stable state shown in Fig. 4(a).

C2: The upper meniscus contacting the top of the tube [Fig. 4(b)]

In this case, the catalyst particle is sitting atop the tube with the upper interface contacting with the top of the tube and the lower interface contacting with the inner corner (see Fig. 4(b)). According to the analysis in Appendix: C2, if

$$(\bar{R}, \rho) \in \{(\bar{R}, \rho) \mid \rho[v(\theta_Y) \tan^3(\pi - \theta_Y) + v(\theta_Y - \frac{\pi}{2})]^{\frac{1}{3}} \leq \bar{R} \leq [v(\theta_Y) + \rho^3 v(\frac{\pi}{2} - \cos^{-1}(\rho \sin \theta_Y))]^{\frac{1}{3}}, 0 \leq \rho \leq \cot(\pi - \theta_Y)\} \quad (27)$$

for $\pi/2 < \theta_Y \leq 3\pi/4$ (see Fig. 9(a) as a representative case) and

$$(\bar{R}, \rho) \in \{(\bar{R}, \rho) \mid \rho[v(\theta_Y) + v(\pi - \theta_Y)]^{\frac{1}{3}} \leq \bar{R} \leq [v(\theta_Y) + \rho^3 v(\frac{\pi}{2} - \cos^{-1}(\rho \sin \theta_Y))]^{\frac{1}{3}}, 0 \leq \rho \leq 1\} \quad (28)$$

for $3\pi/4 < \theta_Y < \pi$ (see Fig. 9(b) as a representative case), there always exist a stable state at $r = R$, which implies that the upper and the lower interfaces have the same curvature, and ϕ is in the admissible angle range shown in Eq. (3). Here, the contact angle between the upper meniscus and the top side is θ_Y whereas the contact angle between the lower meniscus and the inner wall is ϕ , see Fig. 4(b).

C3: The upper meniscus contacting the inner edge of the tube [Fig. 4(c)]

In this case, the particle is sitting atop the tube with both the upper interface and the lower interface contacting with the inner edge of the tube (see Fig. 4(c)). According to the analysis in Appendix: C3, if

$$(\bar{R}, \rho) \in \{(\bar{R}, \rho) \mid [v(\theta_Y - \frac{\pi}{2}) + v(\frac{3\pi}{2} - \theta_Y)]^{\frac{1}{3}} \rho \leq \bar{R} \leq \rho[v(\theta_Y) + v(\pi - \theta_Y)]^{\frac{1}{3}}, 0 \leq \rho \leq 1\} \quad (29)$$

for $3\pi/4 < \theta_Y < \pi$ (see Fig. 9(b) as a representative case), there always exist a stable state at $r = R$, which implies that the upper and the lower interfaces have the

same curvature (i.e., $\theta_i + \phi = 3\pi/2$), and ϕ and θ_i are in the admissible angle range. Here, the contact angle between the upper meniscus and the top side is θ_i whereas the contact angle between the lower meniscus and the inner wall is ϕ , see Fig. 4(c). Notice that this state only exists when $R_I/R_o > 0$ as shown in Fig. 9(b).

Second summary

- (a) All stable states of catalysts in different growth modes are identified as functions of $(\rho, \bar{R}, \theta_Y)$.
- (b) Further evolution pathways of catalyst particles for the cases in Fig. 5, 5(b), 6, 7 and 8 are identified.
- (c) The results for configuration C1 and C2 in Eq. (25), (26), (27) and (28) are consistent with the discussion for stable states of catalyst droplets on a (solid) nanowires in VLS nanowire growth [16].

D. Conclusions

In this paper, surface-energy minimization is used to investigate the mechanisms leading to each state of the catalyst in the tip-growing process and the relation between the properties of the catalyst particles and the morphology of nanotubes.

- (a). The catalyst particle cannot (energetically) detach from the substrate unless it is subject to some external perturbation (not considered herein). This

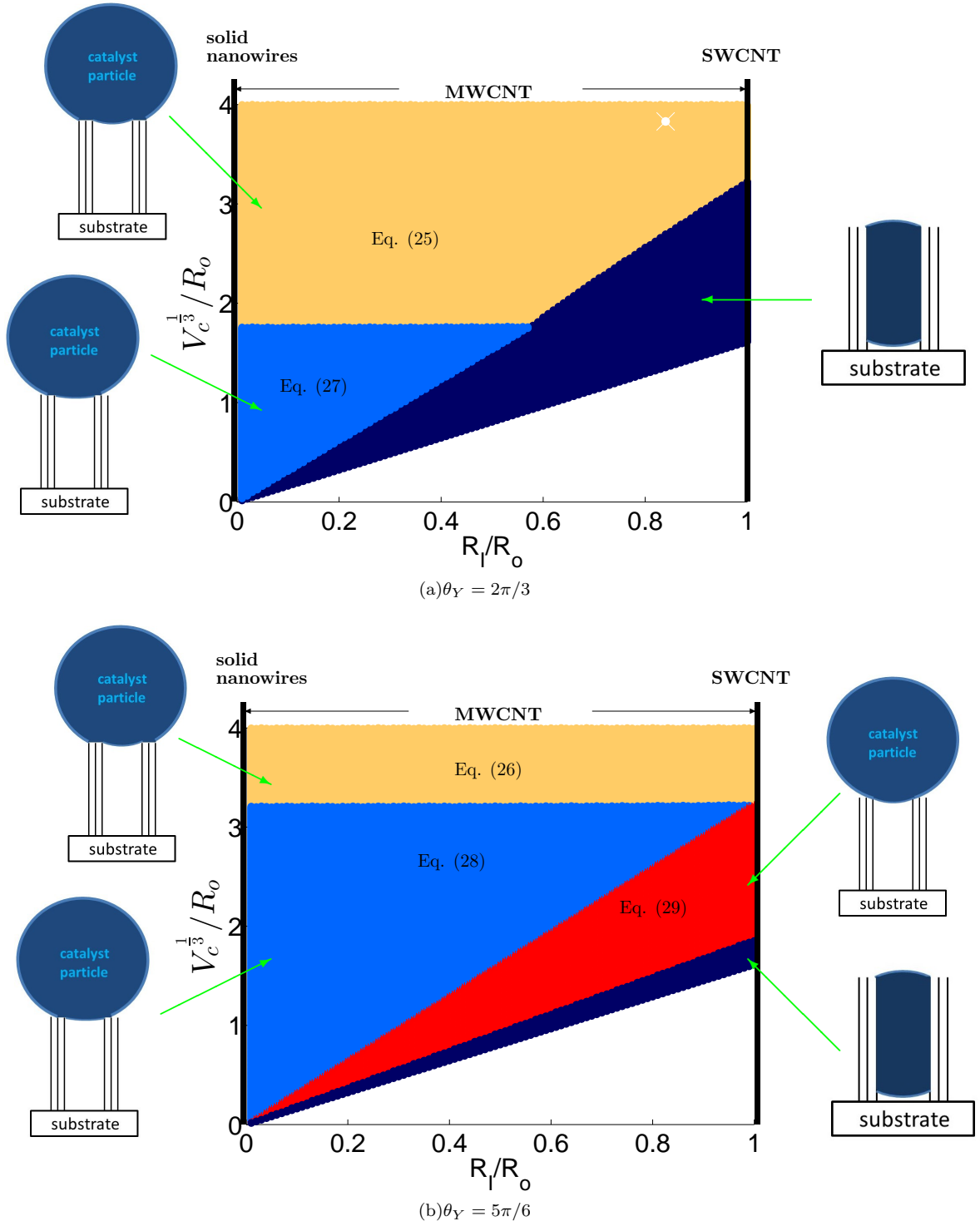


FIG. 9. $(R_I/R_o, V_c^{1/3}/R_o) = (\rho, \bar{R})$ map of having stable state for different possible configurations shown in Fig. 4. (a) $\theta_Y = 2\pi/3$ is taken as the representative case for $\pi/2 < \theta_Y \leq 3\pi/4$. The white point represents the reference case. (b) $\theta_Y = 5\pi/6$ is taken as the representative case for $3\pi/4 < \theta_Y < \pi$.

is consistent with most experimental observations of CNT's that the adhesion force between the catalyst particle and the substrate influences the growth mode (tip-growth or base growth).

(b). Steady “pear-like” shapes of the catalyst particle are always *unstable*.

(c). There are only four possible stable equilibrium

states for a catalyst particle on a tube. They are C1, C2, C3 and E shown in Fig. 4.

(d). In Figs. 9(a) and 9(b), it is seen that the volume of the particle significantly influences the configuration of the tube. For example, if one considers a single-wall tube with radius R_o , the size of the particle has to be larger than $[v(\theta_Y - \pi/2) + v(3\pi/2 - \theta_Y)]^{\frac{1}{3}} R_o$ for it to sit atop the tube. Conversely, given the volume V_c of the particle, in order for the growth process to continue, the size of the tube cannot exceed $V_c^{\frac{1}{3}} / [v(\theta_Y - \pi/2) + v(3\pi/2 - \theta_Y)]^{\frac{1}{3}}$. If the size of the tube exceeds this value, the catalyst particle will be encapsulated in the tube.

(e). It is possible to have the stable state shown as state E in Fig. 4(d) with $\theta_i = \theta_Y - \pi/2$ as long as

$$V_c \geq \frac{4\pi}{3} R_I^3.$$

It is worth noting that this region includes those of C1, C2 or C3 (see Fig. 4(a), 4(b), 4(c)) mentioned above. For the value of $(V_c^{\frac{1}{3}}/R_o, R_I/R_o)$ in those regions, the stable state of the particle depends on its initial state, as shown previously.

(f). Finally, the values of $V_c^{\frac{1}{3}}/R_o$ with energy stable configurations C1 and C2 (for the case of isotropic solid-liquid interface energy) when $R_I/R_o = 0$ shown in Fig. 9(a) and 9(b) are consistent with the results of stable states of catalyst droplet on a (solid) nanowire in VLS nanowire growth in [16].

ACKNOWLEDGMENTS

This research was supported by the Office of Naval Research under Grant no. N00014-14-1-0697.

APPENDIX: ADMISSIBLE ANGLE RANGES

If the upper surface of the catalyst particle is pinned at the outer edge of the tube with angle θ , see Fig. 2(b), the admissible range of θ is

$$\theta_Y \leq \theta \leq \theta_Y + \frac{\pi}{2} \quad (30)$$

as derived by J. W. Gibbs [18]. Similarly, if the lower surface of the catalyst particle is pinned at the inner edge of the tube with angle ϕ as shown in Fig. 2(b), the admissible range of ϕ , according to Gibbs, is

$$\theta_Y - \frac{\pi}{2} \leq \phi \leq \theta_Y. \quad (31)$$

The derivation of (30) and (31) are the same as that in [19]. Similar principles and derivations can be found in [16] and [20].

It is notice that $\theta_Y \leq \pi/2$ is impossible for tip-growth. If $\theta_Y \leq \pi/2$, i.e., the catalyst partially wets the tube, $\phi \leq \pi/2$ according to Eq. (31), it is not possible at equilibrium for the upper surface to contact the outer edge (as shown in Fig. 10(a)) or the top of the tube. To see this, use the Young-Laplace equation,

$$\Delta p = \gamma\kappa, \quad (32)$$

where Δp is the pressure difference across the interface between the catalyst and the vapor. If the upper interface contacts the outer edge or the top of the tube, then the curvatures of the upper and lower interfaces would have opposite signs, which implies there is pressure gradient within the catalyst particle inconsistent with equilibrium. Thus, the only possible equilibrium state has both the upper and the lower interfaces in contact with the inner wall of the tube with the contact angles as shown in Fig. 10(b).

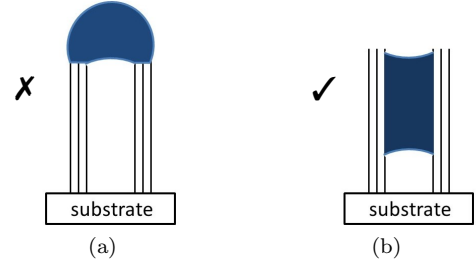


FIG. 10. (a) The upper surface of the catalyst particle contacts the outer edge, whereas the lower surface contacts the inner edge or inner wall of the tube. This configuration is not possible at equilibrium when $\theta_Y \leq \pi/2$. (b) The catalyst particle is totally encapsulated within the tube. Both the upper and the lower interfaces contact the inner wall of the tube with contact angle θ_Y . This is a possible equilibrium state when $\theta_Y \leq \pi/2$.

If $\theta_Y > \pi/2$, the droplet cannot pin on the edge of outlet of the carbon nanotube with angles larger than $\pi/2$, i.e., $\pi < \theta < \theta_Y + \pi/2$ (as shown in Fig. 11(a)) because the meniscus must have constant curvature. similarly to the discussion for the cases $\theta_Y \leq \pi/2$, it is not possible that $\theta_Y - \pi/2 < \phi < \pi/2$ (as shown in Fig. 11(b)) because of the limitation of the Young-Laplace equation. Therefore, if $\theta_Y > \pi/2$, the admissible angle ranges of θ and ϕ are

$$\theta_Y \leq \theta \leq \pi, \quad (33)$$

$$\frac{\pi}{2} \leq \phi \leq \theta_Y. \quad (34)$$

APPENDIX: C1

In this case, the catalyst particle is sitting atop the CNT with the upper interface contacting with the outer

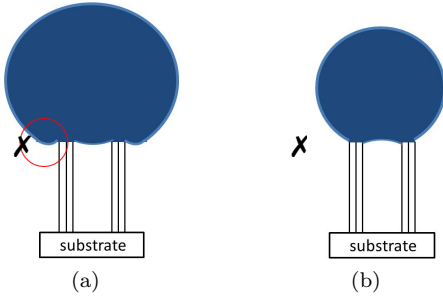


FIG. 11. (a) The upper surface of the catalyst particle dips below the contact point of the upper surface and the outer edge. This configuration is not possible at equilibrium when $\theta_Y > \pi/2$. (b) The upper surface of the catalyst particle contacts the outer edge of the tube whereas the lower surface of the catalyst particle contacts the inner edge of the tube with $\phi < \pi/2$. This configuration is not possible at equilibrium when $\theta_Y > \pi/2$.

edge and the lower interface contacting with the inner edge. The contact angle between the upper interface of catalyst particle and vapor and top is θ whereas the contact angle between the lower interface of the particle and the vapor and the inner wall is ϕ , see Fig. 4(a). This configuration is observed in most tip-growing CNT experiments [7, 8].

Given the size of the CNT and the volume of the catalyst particle, the state of the catalyst particle depends on θ and ϕ and

$$\bar{R}^3(\theta, \phi) = v(\theta) + \rho^3 v(\phi - \frac{\pi}{2}). \quad (35)$$

If $\theta_Y > \pi/2$, the admissible angle ranges of θ and ϕ are

$$\theta_Y \leq \theta \leq \pi, \quad (36)$$

$$\frac{\pi}{2} \leq \phi \leq \theta_Y. \quad (37)$$

The energy of the system is

$$\begin{aligned} \mathcal{E}(\theta, \phi) = & 2\pi \left[\frac{1}{1 + \cos \theta} + \rho^2 \frac{1}{1 + \sin \phi} \right] \\ & + 2\pi \frac{\gamma_{SV}}{\gamma_{LV}} (1 + \rho) \frac{H}{R_o} + \pi \frac{\gamma_{SL}}{\gamma_{LV}} [1 - \rho^2], \end{aligned}$$

where the first term on the left is the energy on the meniscus and the second and third terms represent the energy on the walls. Because the volume of the catalyst particle is conserved,

$$0 = \frac{d\bar{R}^3}{d\phi} = -\pi \frac{(1 - \cos \theta)^2}{\sin^4 \theta} \frac{d\theta}{d\phi} - \pi \rho^3 \frac{(1 - \sin \phi)^2}{\cos^4 \phi} \quad (38)$$

and

$$\frac{d\mathcal{E}}{d\phi} = 2\pi \frac{(1 - \cos \theta)^2}{\sin^3 \theta} \frac{d\theta}{d\phi} + 2\pi \rho^2 \frac{(1 + \sin \phi)^2}{\cos^3 \phi}. \quad (39)$$

Substitute Eq. (38) into Eq. (39) to find that

$$\frac{d\mathcal{E}}{d\phi} = 2\pi \rho^2 \frac{(1 - \sin \phi)^2}{\cos^3 \phi} \left(1 - \frac{r}{R}\right),$$

where $R(= R_o/\sin \theta)$ and $r(= R_I/\cos(\pi - \phi))$ are the radii of the spheres represent the upper and the lower interfaces, respectively. It is obvious that

$$\frac{d\mathcal{E}}{d\phi} = 0, \text{ when } R = r.$$

Moreover,

$$\frac{d^2\mathcal{E}}{d\phi^2} \geq 0, \text{ at } R = r.$$

Thus, at equilibrium, $r = R$ which implies that the upper and the lower interfaces have the same curvature. This is not sufficient for a stable equilibrium. It is possible that either ϕ or θ is not in the admissible range when $r = R$. For example, Fig. 12(a) shows the energy profile via changes of the angle ϕ [θ is determined by ϕ according to Eq. (35)] when $V_c^{1/3}/R_o = 2$ and $R_I/R_o = 0.5$. The minimum point is at around $\phi_0 = 5\pi/8$ ($\theta_0 = 0.714\pi$). If $\theta_Y < \phi_0$, ϕ_0 is outside of the admissible angle range which implies that the catalyst particle cannot pin at the inner corner after reaching $\phi = \theta_Y$. Thus, instead of staying at the state shown in Fig. 4(a), it will evolve to that shown in Fig. 3(a). If $\phi_0 \leq \theta_Y \leq \theta_0$, then the particle will reach a local minimum state shown in Fig. 4(a) with $\phi = \phi_0$ ($\theta = \theta_0$). If $\theta_0 < \theta_Y$, θ_0 is out of the admissible angle range which implies that the catalyst particle cannot pin at the outer corner after reaching $\theta = \theta_Y$. Thus, instead of staying at the state shown in Fig. 4(a), it evolves to that shown in Fig. 4(b). In the other cases, it is also possible that $\theta_0 < \theta_Y < \phi_0$ which implies that both ϕ_0 and θ_0 are outside of admissible ranges. Thus, instead of staying at the state shown in Fig. 4(a), it will evolve to that shown in Fig. 3(b) or 4(d) when the volume of the catalyst particle is not large enough.

According to the analysis above, the regime of (\bar{R}, ρ) having a stable state shown in Fig. 4(a) is given by the intersection of the two regimes. One is

$$\bar{R} \geq [v(\theta_Y) + \rho^3 v(\frac{\pi}{2} - \cos^{-1}(\rho \sin \theta_Y))]^{\frac{1}{3}}.$$

This is because

$$\frac{d\mathcal{E}}{d\theta} < 0,$$

at $\theta = \theta_Y$, when $\phi > \pi - \cos^{-1}(\rho \sin \theta_Y)$. The other one is

$$\bar{R} \geq [v(\pi - \sin^{-1}(-\cos \theta_Y/\rho)) + \rho^3 v(\theta_Y - \frac{\pi}{2})]^{\frac{1}{3}}.$$

This is because

$$\frac{d\mathcal{E}}{d\phi} < 0,$$

at $\phi = \theta_Y$, when $\theta > \pi - \sin^{-1}(-\cos \theta_Y/\rho)$.

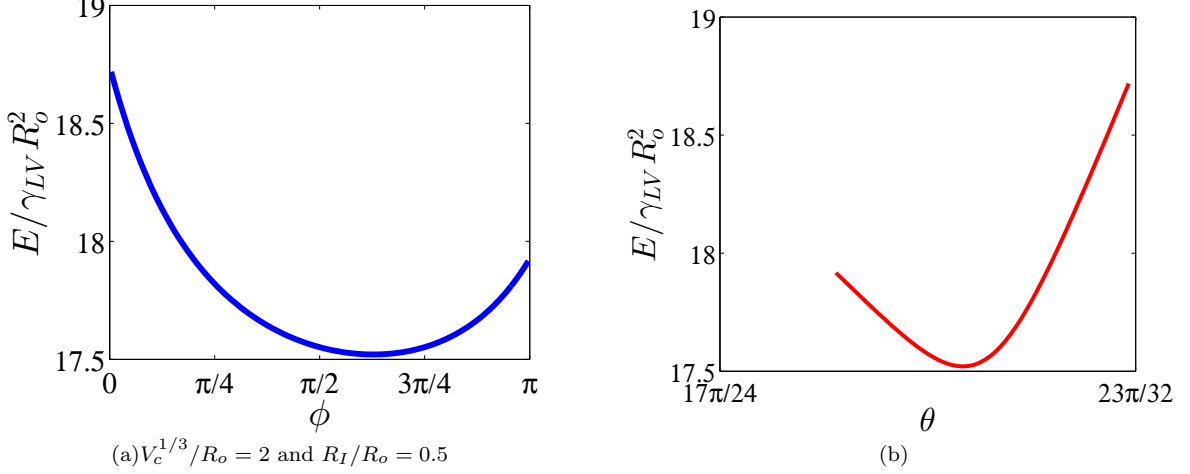


FIG. 12. (a) Relative total energy $[E/\gamma_{LV}R_o^2 = (E_{total} - 2\pi\gamma_{SV}(R_I + R_o)H - \pi\gamma_{SL}(R_o^2 - R_I^2))/\gamma_{LV}R_o^2]$ profile versus ϕ . (b) Relative total energy $[E/\gamma_{LV}R_o^2 = (E_{total} - 2\pi\gamma_{SV}(R_I + R_o)H - \pi\gamma_{SL}(R_o^2 - R_I^2))/\gamma_{LV}R_o^2]$ profile versus θ .

APPENDIX: C2

In this case, the catalyst particle is sitting atop the CNT with the upper interface contacting with the top of the CNT and the lower interface contacting with the inner corner. The contact angle between the upper interface of catalyst particle and vapor and top side is θ_Y whereas the contact angle between the lower interface of the catalyst particle and the vapor and the inner wall is ϕ , see Fig. 4(b). The distance between the contact point of the upper interface with the top side and the inner corner is d_i .

Given the dimensions of the CNT and the volume of the particle, the state of the particle depends on d_i and ϕ and

$$\bar{R}^3(\bar{d}_i, \phi) = (\rho + \bar{d}_i)^3 v(\theta_Y) + \rho^3 v(\phi - \frac{\pi}{2}). \quad (40)$$

The energy of the system is

$$\begin{aligned} \mathcal{E}(\bar{d}_i, \phi) = & -\pi \cos \theta_Y (\rho + \bar{d}_i)^2 + 2\pi \left[\frac{1}{1 + \cos \theta_Y} (\rho + \bar{d}_i)^2 \right. \\ & \left. + \rho^2 \frac{1}{1 + \sin \phi} \right] + 2\pi \frac{\gamma_{SV}}{\gamma_{LV}} \rho \frac{H}{R_o} - \pi \frac{\gamma_{SL}}{\gamma_{LV}} \rho^2 + \pi \frac{\gamma_{SV}}{\gamma_{LV}}, \end{aligned}$$

where $0 < \bar{d}_i < 1 - \rho$ and $\theta_Y - \pi/2 \leq \phi \leq \theta_Y$. Similarly as in the previous case, we have

$$\frac{d\mathcal{E}}{d\bar{d}_i} = (\rho + \bar{d}_i)^2 \frac{(1 - \cos \theta_Y)(2 + \cos \theta_Y) \cos \phi}{\sin \theta_Y (1 + \cos \theta_Y)} \left(1 - \frac{r}{R}\right).$$

Similarly, at equilibrium, it should be that $r = R$ which implies that the upper and the lower interfaces are in the spheres with the same radius. However, it is also possible that ϕ_0 or $(\bar{d}_i)_0$ are not in admissible ranges when $r = R$. If ϕ_0 is outside of admissible range and $(\bar{d}_i)_0$ is in the admissible range, then the catalyst particle cannot pin

at the inner edge after reaching $\phi = \theta_Y$, so it will evolve to cases shown in Figs. 3(b) and 3(c). Otherwise, if $(\bar{d}_i)_0 < 0$, it will evolve to cases shown in Fig. 4(c) or 3(c). Similarly, if $(\bar{d}_i)_0 > (1 - \rho)$, it will evolve to the discussion in Fig. 4(a) or Fig. 3(a).

According to the analysis above, the regime of $(V_c^{1/3}/R_o, R_I/R_o)$ having a stable state shown in Fig. 4(b) is given by the intersection of the three intervals in the following. One is

$$\bar{R} > \rho [v(\theta_Y) \tan^3(\pi - \theta_Y) + v(\theta_Y - \frac{\pi}{2})]^{1/3},$$

because

$$\frac{d\mathcal{E}}{d\phi} < 0$$

at $\phi = \theta_Y$, which implies $\rho + \bar{d}_i < \rho \tan(\pi - \theta_Y)$. The other one is

$$\bar{R} > \rho [v(\theta_Y) + v(\pi - \theta_Y)]^{1/3},$$

because

$$\frac{d\mathcal{E}}{d\bar{d}_i} < 0,$$

at $\bar{d}_i = 0$ when $\phi > \pi - \cos^{-1}(\sin \theta_Y)$. Similarly to the discussion in case C1,

$$\bar{R} < [v(\theta_Y) + \rho^3 v(\frac{\pi}{2} - \cos^{-1}(\rho \sin \theta_Y))]^{1/3}.$$

This is because

$$\frac{d\mathcal{E}}{d\bar{d}_i} > 0,$$

at $\bar{d}_i = 1 - \rho$ when $\phi < \pi - \cos^{-1}(\sin \theta_Y)$.

APPENDIX: C3

In this case, the particle is sitting atop the CNT with both the upper interface and the lower interface contacting with the inner edge of the CNT. The contact angle between the upper interface of catalyst particle and vapor and top side is θ_i whereas the contact angle between the lower interface of the catalyst particle and the vapor and the inner wall is ϕ , see Fig. 4(c).

Given the size of the carbon nanotube and the volume of the catalyst particle, the state of the catalyst particle depends on θ_i and ϕ and

$$\bar{R}^3(\theta_i, \phi) = \rho^3 v(\theta_i) + \rho^3 v(\phi - \frac{\pi}{2}). \quad (41)$$

The energy of the system is

$$\begin{aligned} \mathcal{E}(\theta_i, \phi) = & 2\pi \left[\frac{1}{1 + \cos \theta_i} \rho^2 + \rho^2 \frac{1}{1 + \sin \phi} \right] \\ & + 2\pi \frac{\gamma_{SV}}{\gamma_{LV}} (1 - \rho) \frac{H}{R_o} + \pi \frac{\gamma_{SV}}{\gamma_{LV}} (1 - \rho^2), \end{aligned}$$

where $\theta_Y - \pi/2 \leq \phi, \theta_i \leq \theta_Y$. Similarly to the derivation in last section, we have

$$\begin{aligned} \frac{d\mathcal{E}}{d\phi} &= \rho^2 \frac{(1 - \sin \phi)^2}{\cos^3 \phi} \left(1 - \frac{r}{R}\right) \\ &= \rho^2 \frac{(1 - \sin \phi)^2}{\cos^3 \phi} \left(1 - \frac{\sin \theta_i}{-\cos \phi}\right). \end{aligned}$$

Similarly to the conclusions in case A and B, at equilibrium, $r = R$ which implies that $\theta_i + \phi = 3\pi/2$. Moreover,

$$\frac{d^2\mathcal{E}}{d\phi^2} > 0, \text{ when } \theta_i + \phi = 3\pi/2.$$

Thus, it is a local minimum state under this condition. In addition, considering the admissible angle range, it is possible to have the stable state shown in Fig. 4(c) only when $\theta_Y \geq 3\pi/4$. It is also possible that ϕ_0 or $(\theta_i)_0$ is not in the admissible range when $r = R$. If ϕ_0 is outside of the admissible range then $(\theta_i)_0$ must be in the admissible range which implies that particle cannot pin at the inner edge after reaching $\phi = \theta_Y$; it will evolve to case shown in Fig. 3(c). Otherwise, if θ_0 is outside of the admissible angle range and ϕ_0 is in the admissible range, it will return to cases shown in Fig. 4(a) and 4(b)). According to the analysis above, the regime of $(V_c^{1/3}/R_o, R_I/R_o)$ having a stable state shown in Fig. 4(c) is given by the intersection of the two intervals in the following.

$$\bar{R} > \rho \left[v \left(\frac{3\pi}{2} - \theta_Y \right) + v \left(\theta_Y - \frac{\pi}{2} \right) \right]^{\frac{1}{3}},$$

because

$$\frac{d\mathcal{E}}{d\phi} < 0,$$

at $\phi = \theta_Y$, when $\theta_i > \pi - \sin^{-1}(-\cos \theta_Y)$. The line between gold region (or dark blue region) and blue region is

$$\bar{R} < \rho \left[v(\theta_Y) + v(\pi - \theta_Y) \right]^{\frac{1}{3}}$$

because

$$\frac{d\mathcal{E}}{d\theta_i} < 0,$$

at $\theta_i = \theta_Y$, when $\phi < \pi - \cos^{-1}(\sin \theta_Y)$.

-
- [1] Loiseau, A.; Launois, P.; Petit, P.; Roche, S.; Salvétat, J. P. Understanding carbon nanotubes: from basics to applications. Springer, Lecture Notes in Physics **2006**, 677.
- [2] Kumar, Mukul(2011). Carbon Nanotube Synthesis and Growth Mechanism, Carbon Nanotubes - Synthesis, Characterization, Applications, Dr. Siva Yellampalli (Ed.), ISBN: 978-953-307-497-9, InTech, Available from: <http://www.intechopen.com/books/carbon-nanotubes-synthesis-characterization-applications/carbonnanotube-synthesis-and-growth-mechanism>
- [3] Chiodarelli, N.; Richard, O.; Bender, H.; Heyns, M.; Gendt, S. D.; Groeseneken, G.; Vereecken, P. M. Carbon **2012**, 50, 1748-1752.
- [4] Fiawoo, M.-F. C.; Bonnot, A.-M.; Amara, H.; Bichara, C.; Thibault-Pénisson, J. and Loiseau, A. Phys. Rev. Lett. **2012**, 108, 195503.
- [5] Gohiera, A.; Ewels, C.P.; Minea, T.M.; Djouadi, M.A. Carbon **2008**, 46, 1331-1338.
- [6] Schebarchov, D. and Hendy, S. C. Nano Lett. **2008**, 8, 2253-2257.
- [7] Helveg, S.; López-Cartes, C.; Sehested, J.; Hansen, P. L.; Clausen, B. S., Rostrup-Nielsen, J. R.; Abild-Pedersen, F. and Nørskov, J. K. Nature **2004**, 427, 426-429.
- [8] Hofmann, S.; Sharma, R.; Ducati, C.; Du, G.; Mattevi, C.; Cepek, C.; Cantoro, M.; Pisana, S.; Parvez, A.; Cervantes-Sodi, F.; Ferrari, A. C.; Dunin-Borkowski, R.; Lizzit, S.; Petaccia, L.; Goldoni, A. and Robertson, J. Nano Lett. **2007**, 7, 602-608.
- [9] Moseler, M.; Cervantes-Sodi, F.; Hofmann, S.; Csanyi, G. and Ferrari, A. C. ACS Nano **2010**, 4, 7587-7595.
- [10] Yoshida, H.; Takeda, S.; Uchiyama, T.; Kohno, H. and Homma, Y. Nano Lett. **2008**, 8, 2082-2086.
- [11] Marmur A. J. Colloid and Interface Science **1988**, 122, 209-219.
- [12] Schebarchov, D. and Hendy, S. C. Phys. Rev. E **2008**, 8, (046309)1-6.
- [13] Schebarchov, D. and Hendy, S. C. Nanoscale **2011**, 3, 134-141.
- [14] Willmott, G. R.; Neto, C. and Hendy, S. C., Soft Matter **2011**, 7, 2357-2363.

- [15] Yue, P.; Renardy, Y. *Phys. Fluids* **2013**, 25, (052104)1-19.
- [16] Roper, S. M.; Anderson, A. M.; Davis, S. H. and Voorhees, P. W. *J. Appl. Phys.* **2010**, 107, 114320.
- [17] Hofmann, S.; Blume, R.; Wirth, C.T.; Cantoro, M.; Sharma, R.; Ducati, C.; Hävecker, M.; Zafeiratos, S.; Schnoerch, P.; Oestereich, A.; Teschner, D.; Albrecht, M.; Knop-Gericke, A.; Schlögl, R.; and Robertson, J., J. *Phys. Chem. C*, **2009**, 113 (5), 1648-1656.
- [18] Gibbs, J. W. "Scientific Papers," Vol. 1., 326(1906). Dover, New York, 1961.
- [19] Dyson, D. C., *The Phys. fluids* **1988**, 31, 229-232.
- [20] Oliver, J. F.; Huh, C. and Mason, G. J. *Colloid Interface Sci.* **1977**, 59, 568-581.